Coherent spin manipulation in an exchange-only qubit

E. A. Laird,[1,*] J. M. Taylor,[2] D. P. DiVincenzo,[3] C. M. Marcus,[1] M. P. Hanson,[4] and A. C. Gossard[4]
[1]*Department of Physics, Harvard University, Cambridge, Massachusetts 02138, USA*
[2]*National Institute of Standards and Technology, Gaithersburg, Maryland 20899, USA*
[3]*IBM T. J. Watson Research Center, Yorktown Heights, New York 10598, USA*
[4]*Materials Department, University of California, Santa Barbara, California 93106, USA*
(Received 3 May 2010; revised manuscript received 12 July 2010; published 4 August 2010)

Initialization, two-spin coherent manipulation, and readout of a three-spin qubit are demonstrated using a few-electron triple quantum dot. The three-spin qubit is designed to allow all operations for full qubit control to be tuned via nearest-neighbor exchange interaction. Fast readout of charge states takes advantage of multiplexed reflectometry. Decoherence measured in a two-spin subspace is found to be consistent with predictions based on gate voltage noise with a uniform power spectrum. The theory of the exchange-only qubit is developed and it is shown that initialization of only two spins suffices for operation. Requirements for full multi-qubit control using only exchange and electrostatic interactions are outlined.

DOI: 10.1103/PhysRevB.82.075403 PACS number(s): 73.21.La, 03.67.Lx

I. INTRODUCTION

Electron spins confined in quantum dots are an attractive basis for quantum computing because of their long coherence times and potential for scaling.[1–3] In the simplest proposal,[1] single spins form the logical basis, with single-qubit operations via spin resonance.[4] An alternative scheme, with logical basis formed from singlet and triplet states of two spins[3,5,6] requires inhomogeneous static magnetic field for full single-qubit control.[7] Using three spins to represent each qubit removes the need for an inhomogeneous field; exchange interactions between adjacent spins suffice for all one- and two-qubit operations.[2,8] In this paper, we experimentally demonstrate coherent spin manipulation within a two-spin subspace of a three- spin qubit defined in a triple quantum dot. This operation constitutes a rotation around one of the two exchange-controlled axes in the qubit state space. We demonstrate initialization, one-axis rotation, and readout using one of two charge sensors, monitored by a multiplexed reflectometry circuit.[9,10] Gate noise is estimated based on decoherence rates.

The interactions of three spins have been explored experimentally[11] and theoretically[12] in the context of physical chemistry, where the recombination of two radicals, originally in an unreactive triplet state, can be catalyzed by exchange with a third spin. Few-electron triple quantum dots[13–15] have been used to realize charge reconfigurations corresponding to the elementary operations of quantum cellular automata,[16] although tunable spin interactions have not yet been demonstrated.[17]

II. DEVICE AND MEASUREMENT SCHEME

We first demonstrate how our device [Fig. 1(a)] can be operated in the three- electron regime, then discuss coherent manipulation of the three-spin system. The device was fabricated by patterning Ti/Au topgates on a GaAs/AlGaAs heterostructure incorporating a two-dimensional electron gas 110 nm beneath the surface. Depletion gate voltages create a triple quantum dot together with a pair of charge sensing quantum point contacts (QPCs).[18] Gates L and R are connected to coaxial lines allowing rapid voltage pulses to be applied. The device was measured at 150 mK electron temperature in a dilution refrigerator with a magnetic field $B = 100$ mT applied in-plane.

A frequency-multiplexed radio-frequency (RF) reflectometry circuit[9,10] allowed both QPCs to be measured independently with MHz bandwidth [Fig. 1(a)]. Parallel resonant tank circuits incorporating left and right QPCs were formed from nearby inductors $L_L = 910$ nH and $L_R = 750$ nH together with the parasitic capacitances C_L^P and C_R^P of the bond wires. Bias tees coupled to each tank circuit allowed the DC conductances g_L, g_R of left and right QPCs to be measured simultaneously with the reflectance of the RF circuit. As each QPC was pinched off, a separate dip developed in the reflected signal at corresponding resonant frequency $f_{L,R} \approx (2\pi)^{-1}(L_{L,R}C_{L,R}^P)^{-1/2}$ [Fig. 1(b)]. To monitor the charge sensors, two carrier frequencies f_L and f_R were applied to the single coaxial line driving both resonant circuits [Fig. 1(a)]. The reflected signal was amplified using both cryogenic and room temperature amplifiers, then demodulated by mixing with local oscillators and low-pass filtered to yield voltages V_L^{RF} and V_R^{RF} sensitive predominantly to g_L and g_R [Figs. 1(c) and 1(d)]. To suppress back-action and reduce pulse coupling into the readout circuit, the RF carrier was blanked on both signal and return paths except during the readout pulse configuration; no RF was applied to the readout circuit during spin initialization and manipulation.

With g_R tuned to the point of maximum charge sensitivity $g_R \sim 0.4e^2/h$, the configuration of the triple dot was monitored[10] via V_R^{RF}. Sweeping voltages V_L and V_R on gates L and R, the charge stability diagram of the triple dot was mapped out, as shown in Fig. 1(e)]. Dark transition lines are seen to run with three different slopes, corresponding to electrons added to each of the three dots.[13,14] For the most negative voltages, transitions are no longer seen, indicating that the device has been completely emptied. This allows absolute electron occupancies of the three dots to be assigned to each region of the diagram.

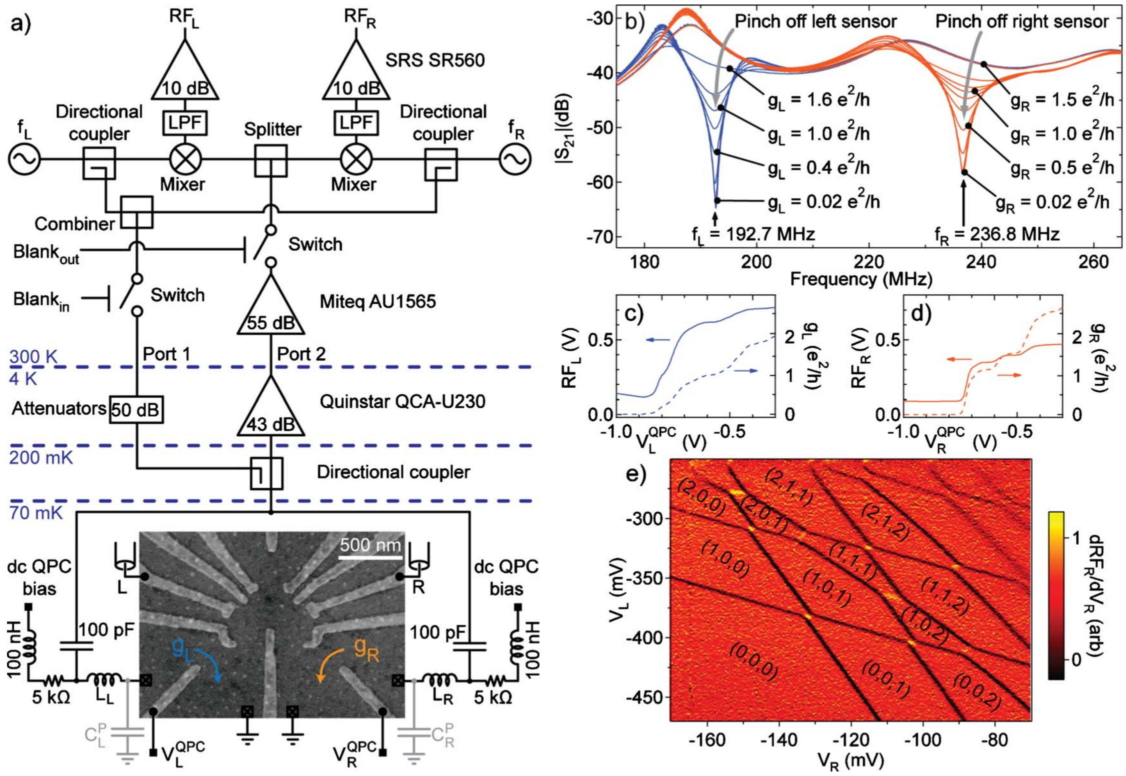

FIG. 1. (Color online) (a) Device and measurement circuit. Patterned topgates define three quantum dots and QPC charge sensors on left and right; voltages applied to gates L and R control the energy levels of the device, while voltages V_L^{QPC} and V_R^{QPC} tune QPC conductances g_L and g_R. The QPCs are incorporated into resonant tank circuits comprising chip inductors L_L and L_R combined with parasitic capacitances C_L^P and C_R^P; bias tees allow the QPCs to be measured both at DC and via RF reflectometry. An RF carrier, generated by combining signals at resonant frequencies f_L and f_R, is applied to the device via a directional coupler; the reflected signal, after amplification, is demodulated by mixing with the original carrier frequencies to yield voltages V_L^{RF} and V_R^{RF} sensitive predominantly to left and right QPCs, respectively. Two RF switches (Minicircuits ZASWA-2-50DR+) allow incident and reflected signals to be blanked except during device readout, reducing backaction and preventing gate pulse coupling to the demodulation circuit. (b) Microwave transmission S_{21} of the cryogenic part of the circuit as a function of frequency, measured between ports 1 and 2 in (a) using a network analyzer. As the QPCs are pinched off, separate resonances develop corresponding to reduced reflection from left and right tank circuits. Carrier frequencies f_L and f_R are chosen to match the two resonance frequencies. (c) and (d), QPC pinchoff measured simultaneously in reflectometry and DC conductance. (e) Reflectometry signal for the right sensor measured as a function of V_L and V_R, showing steps corresponding to charge transitions. Electron configurations for each gate setting are indicated.

III. EXCHANGE-ONLY QUBIT OPERATION

A. Qubit subspace

We work in the subspace of three electrons restricted to occupancies of at most two electrons per dot. To see how exchange can drive arbitrary qubit operations, consider three spins coupled by nearest-neighbor exchange strengths J_{12} and J_{23} [Fig. 2(a)].[2] The eight spin states can be classified by both overall multiplicity and multiplicity of the rightmost spin pair, and comprise a quadruplet, $|Q_{S_z}\rangle$, and two doublets, $|D'_{S_z}\rangle$ and $|D_{S_z}\rangle$, where S_z denotes the z component of total spin and takes values $S_z=\pm 1/2$ or $\pm 3/2$ for the quadruplet and $S_z=\pm 1/2$ for the doublets [Fig. 2(b)].[12,19,20] Whereas for $|D'_{S_z}\rangle$ states, the rightmost pair of spins forms a singlet, for $|D_{S_z}\rangle$ states, the rightmost pair forms a mixture of triplet states (see Appendix B). Alternatively, the doublets can be classified according to the multiplicity of the leftmost pair: States $|\bar{D}'_{S_z}\rangle$ correspond to singlets on the left whereas states $|\bar{D}_{S_z}\rangle$ correspond to triplet states.

The logical basis is formed from two states with equal S_z, one taken from each doublet $|D'_{S_z}\rangle$ and $|D_{S_z}\rangle$. That is, we define the logical qubit states $|0\rangle$ and $|1\rangle$ as $|0\rangle=|D_{\pm 1/2}\rangle$ and $|1\rangle=|D'_{\pm 1/2}\rangle$ (Fig. 1).[2] A valid qubit can be formed from either $S_z=+1/2$ or $S_z=-1/2$ doublet components, or any mixture of the two; it is therefore necessary to prepare and read out only two of the three spins in order to implement full single-qubit operation. We do not discuss further the spin-3/2 subspace, as we start only from states with spin 1/2 and do not otherwise change the total spin.

States of the qubit correspond to points on the Bloch sphere shown in Fig. 2(c). Exchange J_{23} between the rightmost spin pair drives qubit rotations about the vertical axis, exchange J_{12} between the leftmost pair drives rotations about an axis tilted by 120° and defined by doublets $|\bar{D}'_{S_z}\rangle$ and

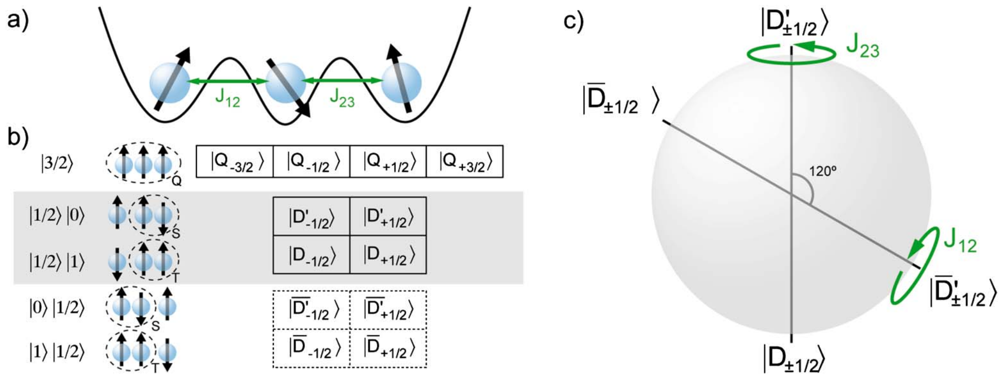

FIG. 2. (Color online) An exchange-only qubit. (a) Electron spins in three adjacent quantum dots are coupled by nearest-neighbor exchange. (b), The eight states of the system can be divided into a quadruplet, Q, and two doublets, D' and D, distinguished by the multiplicity (singlet or triplet) of the rightmost pair of spins. An alternative choice, denoted $\bar{D}$ and $\bar{D}'$, distinguishes the doublets according to the multiplicity of the leftmost spin pair (dashed boxes). (c), Choosing an element from each doublet as the qubit basis [highlighted in (b)], arbitrary unitary transformations are equivalent to rotations on the Bloch sphere shown, where doublet states $|D'_{\pm 1/2}\rangle$ and $|D_{\pm 1/2}\rangle$ correspond to north and south poles and states $|\bar{D}'_{\pm 1/2}\rangle$ and $|\bar{D}_{\pm 1/2}\rangle$ to poles of an axis tilted by 120°. Exchange between middle and right dots drives rotations about the $D-D'$ axis, while exchange between left and middle dots drives rotations about the $\bar{D}-\bar{D}'$ axis. In combination, any rotation can be accomplished.

$|\bar{D}_{S_z}\rangle$. Arbitrary single-qubit operations can be achieved by concatenating up to four exchange pulses.[2]

B. Tuning the exchange interaction

The device energy levels are tuned with an external magnetic field B and by using gate voltages to adjust the energies of different charge configurations (N_L, N_M, N_R), where N_L, N_M, and N_R denote electron occupancies of left, middle and right dots respectively (see Appendix A). Defining detuning ϵ as the energy difference between (2,0,1) and (1,0,2) configurations (in units of gate voltage), three regimes are accessible [Fig. 3(a)]. Neglecting hyperfine coupling, the energy levels are set mainly by the exchange interaction and the Zeeman energy $E_Z = g\mu_B B$, where g is the electron g factor and μ_B is the Bohr magneton. Near $\epsilon=0$, the device is in the (1,1,1) configuration with negligible exchange. As ϵ is increased, hybridization between (1,1,1) and (1,0,2) configurations lowers the energy of $|D'_{S_z}\rangle$ states, until for $\epsilon > \epsilon_+$, the ground state configuration becomes predominantly (1,0,2). An exchange splitting J_{23} for $\epsilon > 0$ prevents occupation of the (1,0,2) configuration with $|Q_{S_z}\rangle$ and $|D_{S_z}\rangle$ spin states and enforces Pauli exclusion in the rightmost dot. Similarly, with decreasing ϵ the energy of $|\bar{D}_{S_z}\rangle$ states is lowered by an amount J_{12}, and below $\epsilon = \epsilon_-$ the ground state configuration becomes predominantly (2,0,1). The various configurations are accessed by tuning gate voltages V_L and V_R coupled predominantly to left and right dots, respectively. The lowest-energy configurations of three capacitively coupled dots are modeled in Fig. 3(b), which also illustrates the detuning axis in gate space.

C. Coherent spin manipulation

Repeated spin state initialization, coherent manipulation, and readout uses the following cycle of voltage pulses[6] on

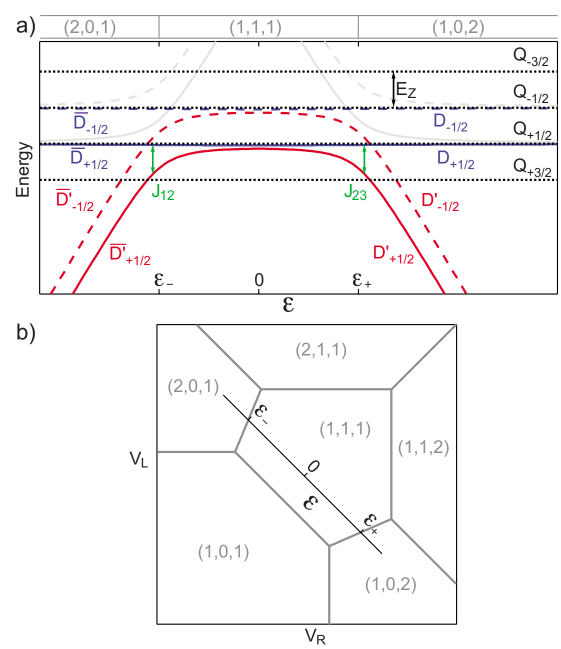

FIG. 3. (Color online) (a) Three-electron energy levels as a function of detuning ϵ, showing Zeeman and exchange splitting (see Appendix A for details of calculation). The case where left and right inter-dot tunnel couplings are equal is plotted; the case of strong asymmetry, corresponding to the experiment, is discussed in Appendix C. Near zero detuning the device is configured in (1,1,1) with negligible exchange; increasing (decreasing) ϵ lowers the energy of the D' $(\bar{D}')$ doublet by exchange $J_{23}(J_{12})$. For $\epsilon > \epsilon_+ (\epsilon < \epsilon_-)$, states in doublet D' $(\bar{D}')$ correspond to a predominant (1,0,2) [(2,0,1)] configuration. Doublet levels corresponding to excited charge configurations are shown as unlabeled light gray lines and play no part in spin manipulation. (b) Ground-state configuration of a triple dot as a function of gate voltages V_L and V_R coupled to left and right dots (Ref. 14). The detuning axis is shown.

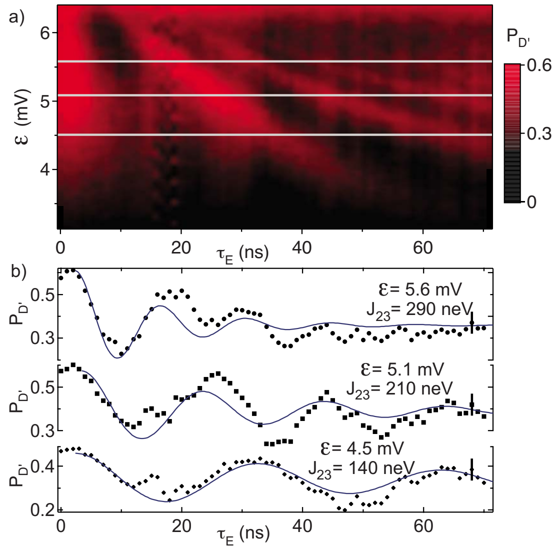

FIG. 4. (Color online) Coherent spin exchange. (a) Probability $P_{D'}$ to return to the initial $|D'_{S_z}\rangle$ state following an exchange pulse sequence, measured as a function of ϵ during the exchange pulse and pulse duration τ_E. Dark and bright regions respectively indicate odd and even numbers of complete spin exchanges. (b), Points: Measured $P_{D'}$ as a function of τ_E for values of ϵ indicated by horizontal lines in (a). Lines: Fits to exponentially damped phase-shifted cosines, corresponding to coherent rotations dephased by electric fields with a white noise spectrum (see text). The fitted exchange $J_{23}(\epsilon)$ for each curve is shown.

gates L and R to rapidly tune ϵ: beginning at $\epsilon > \epsilon_+$ configures the device in (1,0,2) where tunneling to the leads initializes the qubit within the doublet $|D'_{S_z}\rangle$. The detuning is then decreased to $\epsilon \sim 0$ over 1 μs, configuring the device in (1,1,1). Because this ramp time is adiabatic compared to the characteristic hyperfine interaction strength, the spin system enters a ground state defined by the instantaneous nuclear configuration, for example $|\uparrow\downarrow\uparrow\rangle$.[6,21] Pulsing the detuning close to ϵ_+, where J_{23} is large, for a time τ_E leads to coherent exchange of spins between the right-hand dots. Finally, the detuning is ramped back to its original value $\epsilon > \epsilon_+$. The charge configuration is now determined by the outcome of the exchange pulse: Whereas the hyperfine ground state reenters the $|D'_{S_z}\rangle$ doublet in the (1,0,2) configuration, a swapped state such as $|\uparrow\uparrow\downarrow\rangle$ evolves into a superposition of $|D_{S_z}\rangle$ and $|Q_{\pm 1/2}\rangle$ states, causing the device to remain in (1,1,1). At the end of this final ramp, the carrier is unblanked for readout of the charge sensor. Waiting another ~ 5 μs reinitializes the spin state and the cycle begins again.

Averaged over ~ 1000 cycles, the resulting voltage V_R^{RF} is converted to a spin state probability by calibrating it against V_R^{RF} values corresponding to (1,1,1) and (1,0,2) configurations. The probability $P_{D'}$ to return to the initial spin state is shown in Fig. 4(a) as a function of τ_E and ϵ during the exchange pulse. As a function of τ_E, $P_{D'}$ oscillates showing coherent rotation between spin states, and the oscillation frequency, set by $J_{23}(\epsilon)$, increases with ϵ as expected from Fig. 3(a). The measured $P_{D'}(\tau_E)$ is fitted for three values of ϵ with an exponentially damped cosine, corresponding to dephasing by electric fields with a white noise spectrum[6,21] [Fig. 4(b)].

The extracted $J_{23}(\epsilon)$ depends exponentially on ϵ, similar to observations at comparable exchange strength in a double dot,[7] but inconsistent with the power-law dependence found at more negative detunings.[22]

Experimental $P_{D'}(\tau_E)$ values in Fig. 4(b) are fit to an exponentially damped cosine form, $P_{D'}(\tau_E) = Ae^{-\alpha\tau_E}\cos(J_{23}\tau_E/h+\phi)+B$, where α is a damping coefficient reflecting decoherence presumably attributable to gate voltage noise.[21] This form is appropriate for a white noise spectrum, and was chosen over alternative forms (with higher powers of τ_E appearing in the exponent) by the quality of fit, judged by eye. A, B, and ϕ are phenomenological amplitude, offset, and phase parameters. A value for the voltage noise spectral density of detuning, $\sigma_\epsilon = \hbar\alpha^{1/2}/(dJ_{23}/d\epsilon) = 27 \pm 5\ \text{nV}/\sqrt{\text{Hz}}$, was obtained from a fit to the top data set in Fig. 4(b), using an independently measured value $dJ_{23}/d\epsilon$. The lower two curves use the same value of σ_ϵ with independently measured values of $dJ_{23}/d\epsilon$, and show equally good agreement with the data. The origin of this surprisingly large voltage noise, accounting for the observed rapid decoherence, is presently unknown. Reduced contrast ($A<1$) can be attributed to pulse imperfections,[7] which also cause a small phase shift. Similar data for J_{12} could not be obtained in this device due to weak tunnel coupling between left and middle dots (see Appendix C).

In summary, we have fabricated a three-electron spin qubit and demonstrated initialization, coherent spin manipulation using pulsed-gate control of exchange, and state readout. These operations do not yet constitute full qubit control, however. For that, pulsed operation of both J_{12} and J_{23} is needed. Furthermore, to complete a universal set of gates, two-qubit operations will also be needed. That could be done with nearest neighbor exchange coupling of two three-spin qubits, as described in Refs. 2 and 23, which require that the third spin be initialized into a known state. Capacitive coupling of two three- spin qubits can also form a two qubit gate, and does not require initializing the third spin.[3] Those tasks, along with reducing electrical noise to improve coherence, remain for future work.

ACKNOWLEDGMENTS

We acknowledge C. Barthel and D. J. Reilly for discussions. This work was supported by the Department of Defense, IARPA/ARO, the National Science Foundation, and Harvard University.

APPENDIX A: ENERGY LEVELS OF THREE EXCHANGE-COUPLED SPINS

In this Appendix we present the states and energy levels of three electron spins as shown in Fig. 2(a), coupled by nearest-neighbor exchange and subject to a magnetic field. The Hamiltonian is[12]

$$H = J_{12}\left(\mathbf{S}_1\cdot\mathbf{S}_2 - \frac{1}{4}\right) + J_{23}\left(\mathbf{S}_2\cdot\mathbf{S}_3 - \frac{1}{4}\right) - E_Z(S_1^z + S_2^z + S_3^z), \tag{A1}$$

where the spins are denoted $\mathbf{S}_1$, $\mathbf{S}_2$, $\mathbf{S}_3$, the magnetic field is along the z-axis, and units are chosen so that Planck's constant is $\hbar = 1$.

The eight spin eigenstates of the Hamiltonian (A1) form a quadruplet Q and high- and low-energy doublets Δ, Δ',

$$|Q_{+3/2}\rangle = |\uparrow\uparrow\uparrow\rangle, \tag{A2}$$

$$|Q_{+1/2}\rangle = \frac{1}{\sqrt{3}}(|\uparrow\uparrow\downarrow\rangle + |\uparrow\downarrow\uparrow\rangle + |\downarrow\uparrow\uparrow\rangle), \tag{A3}$$

$$|Q_{-1/2}\rangle = \frac{1}{\sqrt{3}}(|\downarrow\downarrow\uparrow\rangle + |\downarrow\uparrow\downarrow\rangle + |\uparrow\downarrow\downarrow\rangle), \tag{A4}$$

$$|Q_{-3/2}\rangle = |\downarrow\downarrow\downarrow\rangle, \tag{A5}$$

$$|\Delta_{+1/2}\rangle = \frac{1}{\sqrt{4\Omega^2 + 2\Omega(J_{12} - 2J_{23})}}((J_{12} - J_{23} + \Omega)|\uparrow\uparrow\downarrow\rangle + (J_{23} - \Omega)|\uparrow\downarrow\uparrow\rangle - J_{12}|\downarrow\uparrow\uparrow\rangle), \tag{A6}$$

$$|\Delta_{-1/2}\rangle = \frac{1}{\sqrt{4\Omega^2 + 2\Omega(J_{12} - 2J_{23})}}((J_{12} - J_{23} + \Omega)|\downarrow\downarrow\uparrow\rangle + (J_{23} - \Omega)|\downarrow\uparrow\downarrow\rangle - J_{12}|\uparrow\downarrow\downarrow\rangle), \tag{A7}$$

$$|\Delta'_{+1/2}\rangle = \frac{1}{\sqrt{4\Omega^2 + 2\Omega(2J_{23} - J_{12})}}((- J_{12} + J_{23} + \Omega)|\uparrow\uparrow\downarrow\rangle - (J_{23} + \Omega)|\uparrow\downarrow\uparrow\rangle + J_{12}|\downarrow\uparrow\uparrow\rangle), \tag{A8}$$

$$|\Delta'_{-1/2}\rangle = \frac{1}{\sqrt{4\Omega^2 + 2\Omega(2J_{23} - J_{12})}}((- J_{12} + J_{23} + \Omega)|\downarrow\downarrow\uparrow\rangle - (J_{23} + \Omega)|\downarrow\uparrow\downarrow\rangle + J_{12}|\uparrow\downarrow\downarrow\rangle),, \tag{A9}$$

with energies

$$E_{Q_{S_z}} = - E_Z S_z, \tag{A10}$$

$$E_{\Delta_{S_z}} = - (J_{12} + J_{23} - \Omega)/2 - E_Z S_z, \tag{A11}$$

$$E_{\Delta'_{S_z}} = - (J_{12} + J_{23} + \Omega)/2 - E_Z S_z, \tag{A12}$$

where $\Omega = \sqrt{J_{12}^2 + J_{23}^2 - J_{12}J_{23}}$. Along the detuning axis of Fig. 3(b), significant charge hybridization is possible between at most pair of dots, allowing the exchange energies to be approximated by functions appropriate for a double dot[21] $J_{12}(\epsilon) = (\epsilon_- - \epsilon)/2 + \sqrt{[(\epsilon_- - \epsilon)/2]^2 + 4t_L^2}$ and $J_{23}(\epsilon) = (\epsilon - \epsilon_+)/2 + \sqrt{[(\epsilon - \epsilon_+)/2]^2 + t_R^2}$, where t_L and t_R are the left and right interdot tunnel couplings. Figure 3(a) shows the resulting energy levels as a function of ϵ for a symmetric device ($t_L = t_R$). [Four additional doublet levels correspond to higher-energy charge configurations not considered in the Hamiltonian (A1).]

APPENDIX B: THE QUBIT BASIS STATES

The qubit basis states are the doublet eigenstates of Hamiltonian (A1) in the limit of vanishing exchange on the left, $J_{12}/J_{23} \to 0$. In this limit, corresponding to the right side of Fig. 3(a), the doublet eigenstates are[2,12]

$$|\Delta_{+1/2}\rangle \to |D_{+1/2}\rangle = \frac{1}{\sqrt{6}}(|\uparrow\uparrow\downarrow\rangle + |\uparrow\downarrow\uparrow\rangle - 2|\downarrow\uparrow\uparrow\rangle), \tag{B1}$$

$$|\Delta_{-1/2}\rangle \to |D_{-1/2}\rangle = \frac{1}{\sqrt{6}}(|\downarrow\downarrow\uparrow\rangle + |\downarrow\uparrow\downarrow\rangle - 2|\uparrow\downarrow\downarrow\rangle), \tag{B2}$$

$$|\Delta'_{+1/2}\rangle \to |D'_{+1/2}\rangle = \frac{1}{\sqrt{2}}(|\uparrow\uparrow\downarrow\rangle - |\uparrow\downarrow\uparrow\rangle), \tag{B3}$$

$$|\Delta'_{-1/2}\rangle \to |D'_{-1/2}\rangle = \frac{1}{\sqrt{2}}(|\downarrow\downarrow\uparrow\rangle - |\downarrow\uparrow\downarrow\rangle), \tag{B4}$$

with energies

$$E_{D_{S_z}} = - E_Z S_z, \tag{B5}$$

$$E_{D'_{S_z}} = - J_{23} - E_Z S_z. \tag{B6}$$

The projection of $|D_{S_z}\rangle$ onto states of the rightmost spins is a mixture of triplet states, whereas the projection of $|D'_{S_z}\rangle$ is a singlet.

Analogously, in the limit of vanishing right-dot exchange $J_{23}/J_{12} \to 0$ (left side of Fig. 3(a)), the eigenstates are elements of the $\bar{D}$ and $\bar{D}'$ doublets, related to D and D' states by interchange of left and right spins,

$$|\Delta_{+1/2}\rangle \to - |\bar{D}_{+1/2}\rangle = - \frac{1}{\sqrt{6}}(|\downarrow\uparrow\uparrow\rangle + |\uparrow\downarrow\uparrow\rangle - 2|\uparrow\uparrow\downarrow\rangle), \tag{B7}$$

$$|\Delta_{-1/2}\rangle \to - |\bar{D}_{-1/2}\rangle = - \frac{1}{\sqrt{6}}(|\uparrow\downarrow\downarrow\rangle + |\downarrow\uparrow\downarrow\rangle - 2|\downarrow\downarrow\uparrow\rangle), \tag{B8}$$

$$|\Delta'_{+1/2}\rangle \to - |\bar{D}'_{+1/2}\rangle = - \frac{1}{\sqrt{2}}(|\uparrow\downarrow\uparrow\rangle - |\downarrow\uparrow\uparrow\rangle), \tag{B9}$$

$$|\Delta'_{-1/2}\rangle \to - |\bar{D}'_{-1/2}\rangle = - \frac{1}{\sqrt{2}}(|\downarrow\uparrow\downarrow\rangle - |\uparrow\downarrow\downarrow\rangle). \tag{B10}$$

The corresponding energies are

$$E_{\bar{D}_{S_z}} = - E_Z S_z, \tag{B11}$$

$$E_{\bar{D}'_{S_z}} = - J_{12} - E_Z S_z. \tag{B12}$$

APPENDIX C: EFFECT OF ASYMMETRIC TUNNEL COUPLINGS

The effect of asymmetric tunnel couplings on the energy levels is shown in Fig. 5 for the case $t_L \ll t_R$. The $\bar{D}'$ levels

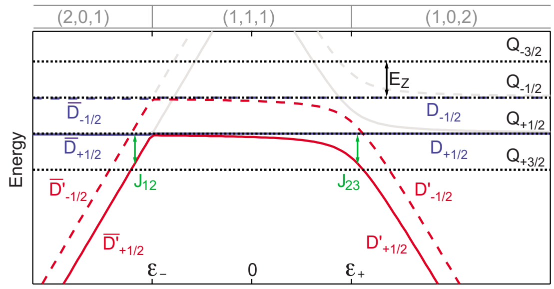

FIG. 5. (Color online) Energy levels of three coupled spins, labeled as in Fig. 3(a), for the case of asymmetric tunnel couplings $t_L \ll t_R$. The divergence of the doublet energy levels on the left becomes much sharper, making the effects of J_{12} difficult to observe.

diverge more abruptly from $\bar{D}$ levels, reducing J_{12} especially for $\epsilon > \epsilon_-$.

A smaller t_L makes the left-dot exchange harder to observe. The simplest pulse cycle used to study the effects of J_{12} began at $\epsilon > \epsilon_+$, configuring the device in (1,0,2) and initializing the qubit within the doublet $|D'_{S_z}\rangle$. The gate voltages were then rapidly pulsed to $\epsilon < 0$ for a time τ_S, during which exchange with the left dot would be expected to drive precession about the $|\bar{D}_{S_z}\rangle - |\bar{D}'_{S_z}\rangle$ axis in Fig. 2(c). For readout, the detuning was returned to $\epsilon > \epsilon_+$, projecting the $|D'_{S_z}\rangle$ component of the spin state into configuration (1,0,2) and projecting $|D_{S_z}\rangle$ into (1,1,1). The resulting $P_{D'}(\tau_S)$, measured via reflectometry voltage V_R^{RF}, showed no coherent oscillations as a function of τ_S; instead a monotonic decay over ~10 ns consistent with hyperfine dephasing[3,6] was observed. This was true with ϵ pulsed to either side of ϵ_- during τ_S.

With energy levels as shown in Fig. 5, this observation can be explained as follows. For appreciable exchange strength J_{12}, ϵ must be pulsed to $\epsilon < \epsilon_-$ during τ_S. However, precession will only take place if, for the $|\bar{D}'_{S_z}\rangle$ component of the spin state, the configuration (2,0,1) can be accessed. If t_L is too small, the transition $(1,1,1) \rightarrow (2,0,1)$ cannot occur within τ_S. Instead, the device enters a metastable (1,1,1) configuration [shown in light gray in Figs. 3(a) and 5], where hyperfine coupling incoherently mixes all three multiplets $|D'_{S_z}\rangle$, $|D_{S_z}\rangle$ and $|Q_{S_z}\rangle$.

*Present address: Kavli Institute of Nanoscience, Delft University of Technology, 2600 GA Delft, The Netherlands.

[1] D. Loss and D. P. DiVincenzo, Phys. Rev. A **57**, 120 (1998).
[2] D. P. DiVincenzo, D. Bacon, J. Kempe, G. Burkard, and K. Whaley, Nature (London) **408**, 339 (2000).
[3] J. M. Taylor, H.-A. Engel, W. Dür, A. Yacoby, C. M. Marcus, P. Zoller, and M. D. Lukin, Nat. Phys. **1**, 177 (2005).
[4] F. H. L. Koppens, C. Buizert, K. J. Tielrooij, I. T. Vink, K. C. Nowack, T. Meunier, L. P. Kouwenhoven, and L. M. K. Vandersypen, Nature (London) **442**, 766 (2006).
[5] J. Levy, Phys. Rev. Lett. **89**, 147902 (2002).
[6] J. R. Petta, A. C. Johnson, J. M. Taylor, E. A. Laird, A. Yacoby, M. D. Lukin, C. M. Marcus, M. P. Hanson, and A. C. Gossard, Science **309**, 2180 (2005).
[7] S. Foletti, H. Bluhm, D. Mahalu, V. Umansky, and A. Yacoby, Nat. Phys. **5**, 903 (2009).
[8] J. Kempe, D. Bacon, D. A. Lidar, and K. B. Whaley, Phys. Rev. A **63**, 042307 (2001).
[9] T. Stevenson, F. Pellerano, C. Stahle, K. Aidala, and R. J. Schoelkopf, Appl. Phys. Lett. **80**, 3012 (2002).
[10] D. J. Reilly, C. M. Marcus, M. P. Hanson, and A. C. Gossard, Appl. Phys. Lett. **91**, 162101 (2007).
[11] E. Step, A. Buchachenko, and N. Turro, J. Am. Chem. Soc. **116**, 5462 (1994).
[12] A. Buchachenko and V. Berdinsky, Chem. Rev. **102**, 603 (2002).
[13] L. Gaudreau, S. A. Studenikin, A. S. Sachrajda, P. Zawadzki, A. Kam, J. Lapointe, M. Korkusinski, and P. Hawrylak, Phys. Rev. Lett. **97**, 036807 (2006).
[14] D. Schröer, A. D. Greentree, L. Gaudreau, K. Eberl, L. C. L. Hollenberg, J. P. Kotthaus, and S. Ludwig, Phys. Rev. B **76**, 075306 (2007).
[15] L. Gaudreau, A. Kam, G. Granger, S. A. Studenikin, P. Zawadzki, and A. S. Sachrajda, Appl. Phys. Lett. **95**, 193101 (2009).
[16] G. Toth and C. S. Lent, Phys. Rev. A **63**, 052315 (2001).
[17] L. Gaudreau, A. S. Sachrajda, S. A. Studenikin, P. Zawadzki, and A. Kam, Physica E (Amsterdam) **40**, 978 (2008).
[18] M. Field, C. G. Smith, M. Pepper, D. A. Ritchie, J. E. F. Frost, G. A. C. Jones, and D. G. Hasko, Phys. Rev. Lett. **70**, 1311 (1993).
[19] E. Knill, R. Laflamme, and L. Viola, Phys. Rev. Lett. **84**, 2525 (2000).
[20] C.-P. Yang and J. Gea-Banacloche, Phys. Rev. A **63**, 022311 (2001).
[21] J. M. Taylor, J. R. Petta, A. C. Johnson, A. Yacoby, C. M. Marcus, and M. D. Lukin, Phys. Rev. B **76**, 035315 (2007).
[22] E. A. Laird, J. R. Petta, A. C. Johnson, C. M. Marcus, A. Yacoby, M. P. Hanson, and A. C. Gossard, Phys. Rev. Lett. **97**, 056801 (2006).
[23] Y. Kawano, K. Kimura, H. Sekigawa, M. Noro, K. Shirayanagi, M. Kitagawa, and M. Ozawa, Quantum Inf. Process. **4**, 65 (2005).